

Graphical Abstract

Adaptable and Interpretable Framework for Anomaly Detection in Streaming Energy Systems

Marek Wadinger, Michal Kvasnica

Highlights

Adaptable and Interpretable Framework for Anomaly Detection in Streaming Energy Systems

Marek Wadinger, Michal Kvasnica

- Combines interpretability with adaptation to change points in single anomaly detection system
- Isolates root cause of anomalies considering relationships between features
- Demonstrates interpretability by providing process limits for each feature
- Provides comparable detection accuracy to established general methods

Adaptable and Interpretable Framework for Anomaly Detection in Streaming Energy Systems

Marek Wadinger^{a,*}, Michal Kvasnica^a

^a*Institute of Information Engineering, Automation and Mathematics, Slovak University of Technology in Bratislava, Radlinskeho 9, Bratislava, 812 37, Bratislava, Slovakia*

Abstract

In this paper, we introduce an Adaptable and Interpretable Framework for Anomaly Detection (AID) designed for streaming energy systems utilizing IoT devices. AID leverages adaptive conditional probability distribution modeling to capture the normal operation of dynamic systems and isolate root causes of anomalies. The framework dynamically updates parameter of multivariate Gaussian distribution, allowing it to adapt to non-stationarity. AID interprets anomalies as significant deviations from conditional probability, encompassing interactions as well as both spatial and temporal irregularities by exposing them as features. Additionally, dynamic process limits are drawn to pinpoint root causes. The framework also alerts individual signal as outliers in sampling. Two real-world case studies showcase AID's capabilities. The first study focuses on Battery Energy Storage Systems (BESS), demonstrating AID's effectiveness in capturing system anomalies, providing less conservative signal limits, and leveraging a physical model for temperature anomaly detection. The second case study delves into monitoring temperature profiles of battery modules, where AID successfully identifies hardware faults, emphasizing its importance in energy storage system safety and profitability. A benchmark evaluation on industrial data shows that AID delivers comparable results to other self-learning adaptable anomaly detection methods, with the added advantage of root cause isolation.

Keywords: Anomaly detection, Root cause isolation, Iterative learning control, Statistical learning, IoT

*

Email address: marek.wadinger@stuba.sk (Marek Wadinger)
URL: uiam.sk/~wadinger (Marek Wadinger)

¹ 1. Introduction

² Anomaly detection systems play a critical role in risk-averse systems by
³ identifying abnormal patterns and adapting to novel expected patterns in
⁴ data. These systems are particularly vital in the context of Internet of Things
⁵ (IoT) devices that continuously stream high-fidelity data to control units.

⁶ In this rapidly evolving field with long-spanning roots, Chandola et al.
⁷ conducted an influential review of prior research efforts across diverse appli-
⁸ cation domains (Chandola et al. (2009)). Recent studies have underscored
⁹ the need for holistic and tunable anomaly detection methods accessible to
¹⁰ operators (Laptev et al. (2015); Kejariwal (2015); Cook et al. (2020)).

¹¹ Cook et al. denote substantial aspects that pose challenges to anomaly
¹² detection in IoT, including the temporal, spatial, and external context of
¹³ measurements, multivariate characteristics, noise, and nonstationarity (Cook
¹⁴ et al. (2020)). To address these complexities, Zhang et al. have successfully
¹⁵ employed spatially distributed sensors and time-relative modulation. Their
¹⁶ approach has proven effective, particularly in the context of complex non-
¹⁷ linear systems, offering potential solutions to some of the challenges posed
¹⁸ by IoT data (Zhang et al. (2024)). Huang et al., on the other hand, tackled
¹⁹ the problems of detecting global outliers, local outliers, and outlier clusters
²⁰ simultaneously. Their proposed approach, based on density estimation, relies
²¹ on the notion that density distributions should exhibit minimal variations in
²² local areas. To achieve this, they introduce a novel turning ratio metric,
²³ which reduces reliance on hyperparameters and enhances anomaly detection
²⁴ (Huang et al. (2023)).

²⁵ Additionally, feature engineering techniques play a crucial role in cap-
²⁶ turing contextual properties and enhancing anomaly detection performance
²⁷ (Fan et al. (2019)). However, it's worth noting that feature engineering may
²⁸ introduce categorical variables and significantly increase dimensionality of
²⁹ the data, requiring specific methods for handling large data, sizeable data
³⁰ storage, and substantial computational resources (Talagala et al. (2021)).
³¹ Recently, Li et al. introduced an attribute-weighted outlier detection algo-
³² rithm, designed for high-dimensional datasets with mixtures of categorical
³³ and numerical data. Their approach assigns different weights to individ-
³⁴ ual attributes based on their importance in anomaly detection and uses
³⁵ these weights to calculate distances between data points. Notably, Li et

al. demonstrated the superior performance of their algorithm compared to state-of-the-art methods (Li and Liu (2024)). Another strategy for handling high-dimensional data involves using deep learning methods with synthetic normal data to enhance the detection of outliers with subtle deviations, as proposed in Du et al. (2024).

Nevertheless, the presence of nonstationarity, often stemming from concept drift (a shift in data patterns due to changes in statistical distribution) and change points (permanent alterations in system state), presents a substantial challenge (Salehi and Rashidi (2018)). In practical scenarios, those changes tend to be unpredictable in both their spatial and temporal aspects. Consequently, they require systems with solid outlier rejection capabilities of intelligent tracking algorithms (Barbosa Roa et al. (2019)). This underscores the critical importance of an anomaly detection method's ability to adapt to evolving data structures, especially in long-term deployments. Nevertheless, as (Tartakovsky et al. (2013)) remarked, the immediate detection is not a feasible option unless there is a high tolerance for false alarms.

The former scalability problem now introduces a significant latency in detector adaptation (Wu et al. (2021)). Incremental learning methods allowed adaptation while restraining the storage of the whole dataset. The supervised operator-in-the-loop solution offered by Pannu et al. showed the detector's adaptation to data labeled on the flight (Pannu et al. (2012)). Others approached the problem as sequential processing of bounded data buffers in univariate signals (Ahmad et al. (2017)) and multivariate systems (Bosman et al. (2015)).

1.1. Related Work

Recent advances in anomaly detection have broadened its scope to include root cause identification governed by the development of explanatory methods capable of diagnosing and tracking faults across the system. Studies can be split into two groups of distinct approaches. The first group approaches explainability as the importance of individual features (Carletti et al. (2019); Nguyen et al. (2019); Amarasinghe et al. (2018)). Those studies allow an explanation of novelty by considering features independently. The second group uses statistical learning creating models explainable via probability. For instance, integration of variational Bayesian inference probabilistic graph neural network allowed Zhang et al. to model the posterior distribution of sensor dependency for gas leakage localization on unlabeled

72 data (Zhang et al. (2023)). Yang et al. recently proposed a Bayesian net-
73 work (BN) for fault detection and diagnosis. In this BN, individual nodes
74 of the network represent normally distributed variables, whereas the multi-
75 ple regression model defines weights and relationships. Using the predefined
76 structure of the BN, the authors propose an offline training with online de-
77 tection and diagnosis (Yang et al. (2022)).

78 Given the infrequent occurrence of anomalies and their potential absence
79 in training data, the incorporation of synthetic data or feature extraction for
80 various detected events emerges to assist diagnosis of the system. Brito et al.
81 designed synthetic faults based on expert knowledge and introduced them
82 into a transfer learning classifier to exploit faults in rotating machinery, with
83 a subsequent explanation layer (Brito et al. (2023)). Conversely, We et al.
84 leveraged feature selection to expose various types of abnormal behavior. The
85 team presents competitive performance while using change in relationships
86 to provide causal inference (Wu et al. (2024)).

87 However, it is crucial to underscore that offline training, as previously em-
88 phasized, is inherently inadequate when it comes to adapting to anticipated
89 novel patterns, rendering it unsuitable for sustained, long-term operation on
90 IoT devices.

91 This paper emphasizes the importance of combining adaptability in in-
92 terpretable anomaly detection and proposes a method that addresses this
93 challenge. Here we report the discovery and characterization of an adaptive
94 anomaly detection method for streaming IoT data. The ability to diag-
95 nose multivariate data while providing root cause isolation, inherent in the
96 univariate case, extends our previous contribution to the field as presented
97 in (Wadinger and Kvasnica (2023)). The proposed algorithm represents a
98 general method for a broad range of safety-critical systems where anomaly
99 diagnosis and identification are paramount.

100 *1.2. Novelty of proposed approach*

101 The idea of using statistical outlier detection is well-established. We high-
102 lighting impactful contributions of (Yamanishi and Takeuchi (2002)) and (Ya-
103 manishi et al. (2004)). The authors propose a method for detecting anomalies
104 in a time series. The method is based on the assumption that the continuous
105 data is generated by a mixture of Gaussian distributions, while discrete data
106 is modeled as histogram density. The authors solve the problem of change
107 point detection as well. However, the adaptation system is unaware of such
108 changes, making the moving window the only source of adaptation. Our

109 self-supervised approach offers intelligent adaptation w.r.t. detected change
110 points. Moreover, the author of the study does not attempt to isolate the
111 root cause of the anomaly. We do so by computing the conditional proba-
112 bility of each measurement given the rest of the measurements and drawing
113 limits defining the normal event probability threshold.

114 A limited number of studies have focused on adaptation and interpretabil-
115 ity within the framework of anomaly detection. Two recent contributions
116 in this area are (Steenwinckel (2018)) and (Steenwinckel et al. (2021)). In
117 (Steenwinckel (2018)), the authors emphasize the importance of combining
118 prior knowledge with a data-driven approach to achieve interpretability, par-
119 ticularly concerning root cause isolation. They propose a novel approach
120 that involves extracting features based on knowledge graph pattern extrac-
121 tion and integrating them into the anomaly detection mechanism. This graph
122 is subsequently transformed into a matrix, and adaptive region-of-interest ex-
123 traction is performed using reinforcement learning techniques. To enhance
124 interpretability, a Generative Adversarial Network (GAN) reconstructs a new
125 graphical representation based on selected vectors. However, it's important
126 to note that the validation of this idealized approach is pending further in-
127 vestigation. Lately, (Steenwinckel et al. (2021)) introduced a comprehen-
128 sive framework for adaptive anomaly detection and root cause analysis in
129 data streams. While the adaptation process is driven by user feedback, the
130 specific mechanism remains undisclosed. The authors present an interpreta-
131 tion of their method through a user dashboard, featuring visualizations of
132 raw data. This dashboard is capable of distinguishing between track-related
133 problems and train-related issues, based on whether multiple trains at the
134 same geographical location approach the anomaly. Meanwhile, our attempts
135 aim to develop a self-supervised method capable of learning without human
136 supervision which is often limited in time and poses significant delays in
137 adaptation, while interpretation offers straightforward statistical reasoning
138 and root cause isolation.

139 *1.3. Validation*

140 Two case studies show that our proposed method, based on dynamic joint
141 normal distribution, has the capacity to explain novelties, isolate the root
142 cause of anomalies, and allow adaptation to change points, advancing recently
143 developed anomaly detection techniques for long-term deployment and cross-
144 domain usage. We observe similar detection performance, albeit with lower
145 scalability, when comparing our approach to well-established unsupervised

146 anomaly detection methods in streamed data which create a bedrock for
147 many state-of-the-art contributions, such as One-Class SVM (Amer et al.
148 (2013); Liu et al. (2014); Krawczyk and Woźniak (2015); Miao et al. (2019);
149 Gözüaçık and Can (2021)), and Half-Space Trees (Wetzig et al. (2019); Lyu
150 et al. (2020)).

151 *1.4. Broader Impact*

152 Potential applications of the proposed method are in the field of energy
153 storage systems, where the ability to detect anomalies and isolate their root
154 cause, whilst adapting to changes in operation and environment, is crucial
155 for the safety of the system. The proposed method is suitable for the existing
156 infrastructure of the system, allowing detection and diagnosis of the system
157 based on existing data streams. The dynamic process limits allow opera-
158 tional metrics monitoring, making potential early detection and prevention
159 easier. Using adaptable methods without interpretability, on the other hand,
160 may pose safety risks and lower total financial benefits, as the triggered false
161 alarms may need to be thoroughly analyzed, resulting in prolonged down-
162 times.

163 The main contribution of the proposed solution to the developed body of
164 research is that it:

- 165 • Enriches interpretable anomaly detection with adaptive capabilities
- 166 • Identifies systematic outliers and root cause
- 167 • Uses self-learning approach on streamed data
- 168 • Utilizes existing IT infrastructure
- 169 • Establishes dynamic limits for signals

170 *1.5. Paper Organization*

171 The rest of the paper is structured as follows: We begin with the prob-
172 lem and motivation in **Section 1**, providing context. Next, in **Section 2**,
173 we lay the theoretical groundwork. Our proposed adaptive anomaly de-
174 tection method is detailed in **Section 3**. We then demonstrate real-world
175 applications in **Section 4**. Finally, we conclude the paper in **Section 5**,
176 summarizing findings and discussing future research directions.

177 **2. Preliminaries**

178 In this section, we present the fundamental ideas that form the basis
179 of the developed approach. Subsection 2.1 explains Welford's online algo-
180 rithm, which can adjust distribution to changes in real-time. Subsection 2.2
181 proposes a two-pass implementation that can reverse the impact of expired
182 samples. The math behind distribution modeling in Subsection 2.3 estab-
183 lishes the foundation for the Gaussian anomaly detection model discussed in
184 Subsection 2.5, followed by conditional probability computation in Subsec-
185 tion 2.4. The last subsection of the preliminaries is devoted to the definition
186 of anomalies.

187 *2.1. Welford's Online Algorithm*

188 Welford introduced a numerically stable online algorithm for calculating
189 mean and variance in a single pass. The algorithm allows the processing
190 of IoT device measurements without the need to store their values Welford
191 (1962).

192 Given measurement x_i where $i = 1, \dots, n$ is a sample index in sample
193 population n , the corrected sum of squares S_n is defined as

$$S_n = \sum_{i=1}^n (x_i - \bar{x}_n)^2, \quad (1)$$

194 with the running mean \bar{x}_n defined as previous mean \bar{x}_{n-1} weighted by pro-
195 portion of previously seen population $n - 1$ corrected by current sample as

$$\bar{x}_n = \frac{n-1}{n} \bar{x}_{n-1} + \frac{1}{n} x_n = \bar{x}_{n-1} + \frac{x_n - \bar{x}_{n-1}}{n}. \quad (2)$$

196 Throughout this paper, we consider the following formulation of an update
197 to the corrected sum of squares:

$$S_n = S_{n-1} + (x_n - \bar{x}_{n-1})(x_n - \bar{x}_n), \quad (3)$$

198 as it is less prone to numerical instability due to catastrophic cancellation.
199 Finally, the corresponding unbiased variance is

$$s_n^2 = \frac{S_n}{n-1}. \quad (4)$$

200 This implementation of the Welford method requires the storage of three
201 scalars: \bar{x}_{n-1} ; n ; S_n .

202 2.2. Inverse Welford's Algorithm

203 Based on (2), it is clear that the influence of the latest sample over the
 204 running mean decreases as the population n grows. For this reason, regulating
 205 the number of samples used for sample mean and variance computation
 206 has crucial importance over adaptation. Given access to the instances used
 207 for computation and expiration period $t_e \in \mathbb{N}_0^{n-1}$, reverting the impact of
 208 x_{n-t_e} can be written as follows

$$S_{n-1} = S_n - (x_{n-t_e} - \bar{x}_{n-1})(x_{n-t_e} - \bar{x}_n), \quad (5)$$

209 where the reverted mean is given as

$$\bar{x}_{n-1} = \frac{n}{n-1}\bar{x}_n - \frac{1}{n-1}x_{n-t_e} = \bar{x}_n - \frac{x_{n-t_e} - \bar{x}_n}{n-1}. \quad (6)$$

210 Finally, the unbiased variance follows the formula:

$$s_{n-1}^2 = \frac{S_{n-1}}{n-2}. \quad (7)$$

211 2.3. Statistical Model of Multivariate System

212 Multivariate normal distribution generalizes the multivariate systems to
 213 the model where the degree to which variables are related is represented by
 214 the covariance matrix. Gaussian normal distribution of variables is a reasonable
 215 assumption for process measurements, as it is a common distribution
 216 that arises from stable physical processes measured with noise. The general
 217 notation of multivariate normal distribution is:

$$\mathbf{X} \sim \mathcal{N}_k(\boldsymbol{\mu}, \boldsymbol{\Sigma}), \quad (8)$$

218 where k -dimensional mean vector is denoted as $\boldsymbol{\mu} = (\bar{x}_1, \dots, \bar{x}_k)^T \in \mathbb{R}^k$
 219 and $\boldsymbol{\Sigma} \in \mathbb{R}^{k \times k}$ is the $k \times k$ covariance matrix, where k is the index of last
 220 random variable.

221 The probability density function (PDF) $f(\mathbf{x}; \boldsymbol{\mu}, \boldsymbol{\Sigma})$ of multivariate normal
 222 distribution is denoted as:

$$f(\mathbf{x}; \boldsymbol{\mu}, \boldsymbol{\Sigma}) = \frac{1}{(2\pi)^{k/2}|\boldsymbol{\Sigma}|^{1/2}} e^{-\frac{1}{2}(\mathbf{x}-\boldsymbol{\mu})^\top \boldsymbol{\Sigma}^{-1}(\mathbf{x}-\boldsymbol{\mu})}, \quad (9)$$

223 where \mathbf{x} is a k -dimensional vector of measurements x_i at time i , $|\boldsymbol{\Sigma}|$
 224 denotes the determinant of $\boldsymbol{\Sigma}$, and $\boldsymbol{\Sigma}^{-1}$ is the inverse of $\boldsymbol{\Sigma}$.

225 The cumulative distribution function (CDF) of a multivariate Gaussian
 226 distribution describes the probability that all components of the random ma-
 227 trix \mathbf{X} take on a value less than or equal to a particular point \mathbf{x} in space,
 228 and can be used to evaluate the likelihood of observing a particular set of
 229 measurements or data points. The CDF is often used in statistical applica-
 230 tions to calculate confidence intervals, perform hypothesis tests, and make
 231 predictions based on observed data. In other words, it gives the probability
 232 of observing a random vector that falls within a certain region of space. The
 233 standard notation of CDF is as follows:

$$F(\mathbf{x}; \boldsymbol{\mu}, \boldsymbol{\Sigma}) = \int_{-\infty}^{\mathbf{x}} f(\mathbf{x}; \boldsymbol{\mu}, \boldsymbol{\Sigma}) d\mathbf{x}, \quad (10)$$

234 where $d\mathbf{x}$ denotes the integration over all k dimensions of \mathbf{x} .

235 As the equation (10) cannot be integrated explicitly, an algorithm for
 236 numerical computation was proposed in Genz (2000).

237 Given the PDF, we can also determine the value of \mathbf{x} that corresponds to a
 238 given quantile q using a numerical method for inversion of CDF (ICDF) often
 239 denoted as percent point function (PPF) or $F(\mathbf{x}; \boldsymbol{\mu}, \boldsymbol{\Sigma})^{-1}$. An algorithm that
 240 calculates the value of the PPF for univariate normal distribution is reported
 241 below as Algorithm 1.

Algorithm 1 Percent-Point Function for Normal Distribution

Input: quantile q , sample mean \bar{x}_n (2), sample variance s_n^2 (4)

Output: threshold value $\tilde{x}_{q,n}$

Initialisation :

1: $f \leftarrow 10; l \leftarrow -f; r \leftarrow f;$

LOOP Process

2: **while** $F(l; \bar{x}_n, s_n^2) > 0$ **do**

3: $r \leftarrow l;$

4: $l \leftarrow lf;$

5: **end while**

6: **while** $F_X(r) - q < 0$ **do**

7: $l \leftarrow r;$

8: $r \leftarrow rf;$

9: **end while**

10: $\tilde{x}_{q,n} = \arg \min_{x_n} \|F(x_n; \bar{x}_n, s_n^2) - q\|$ s.t. $l \leq x_n \leq r$

11: **return** $\tilde{x}_{q,n} \sqrt{s_n^2 + \bar{x}_n}$

242 The Algorithm 1 for PPF computation is solved using an iterative root-
243 finding algorithm such as Brent's method Brent (1972).

244 *2.4. Conditional Probability Distribution*

245 Considering that we observe particular vector \mathbf{x}_i , we can update probability
246 distributions, calculated according to the rules of conditional probability,
247 of individual measurements within the vector given the rest of the measure-
248 ments in \mathbf{x}_i . Let's assume multivariate normal distribution (8) and without
249 loss of generality, that the vector \mathbf{x}_i can be partitioned into subset variable
250 x_a , and complement vector \mathbf{x}_b as follows

$$\mathbf{x}_i = \begin{bmatrix} x_a \\ \mathbf{x}_b \end{bmatrix} \text{ with dimensions } \begin{bmatrix} 1 \times 1 \\ (k-1) \times 1 \end{bmatrix}, \quad (11)$$

251 where $a = 1, \dots, k$ and $\mathbf{b} = \{1, 2, \dots, k\}$ where $a \notin \mathbf{b}$. This partitioning
252 allows us to define block-wise mean and covariance as follows:

$$\boldsymbol{\mu} = \begin{bmatrix} \mu_a \\ \boldsymbol{\mu}_b \end{bmatrix} \text{ with dimensions } \begin{bmatrix} 1 \times 1 \\ (k-1) \times 1 \end{bmatrix}, \quad (12)$$

253 and

$$\boldsymbol{\Sigma} = \begin{bmatrix} \sigma_{aa}^2 & \boldsymbol{\Sigma}_{ab} \\ \boldsymbol{\Sigma}_{ba} & \boldsymbol{\Sigma}_{bb} \end{bmatrix} \text{ with dimensions } \begin{bmatrix} 1 \times 1 & 1 \times (k-1) \\ (k-1) \times 1 & (k-1) \times (k-1) \end{bmatrix}. \quad (13)$$

254 where a and \mathbf{b} represent distinct components within the vector.

255 Subsequently, we can derive the conditional distribution of any subset
256 variable x_a , given the complementary vector \mathbf{x}_b . This conditional distribution
257 conforms to a univariate normal distribution, characterized by:

$$X_a | \mathbf{X}_b \sim \mathcal{N}(\mu_{a|\mathbf{b}}, \sigma_{a|\mathbf{b}}^2). \quad (14)$$

258 where $\mu_{a|\mathbf{b}}$ denotes the conditional mean and $\sigma_{a|\mathbf{b}}^2$ represents the condi-
259 tional variance. These crucial parameters can be computed using the Schur
260 complement.

261 For a general matrix M expressed as:

$$M = \begin{bmatrix} A & B \\ C & D \end{bmatrix}, \quad (15)$$

262 the Schur complement of the block matrix M is denoted as:

$$M \mid D = A - BD^{-1}C. \quad (16)$$

263 Applying Equation (16), we can calculate the conditional variance $\sigma_{a|b}^2$
 264 using the covariance matrix notation from Equation (13) as follows:

$$\sigma_{a|b}^2 = \sigma_{aa}^2 - \Sigma_{ab}\Sigma_{bb}^{-1}\Sigma_{ba}, \quad (17)$$

265 while the conditional mean, denoted as $\mu_{a|b}$, is determined by:

$$\mu_{a|b} = \mu_a + \Sigma_{ab}\Sigma_{bb}^{-1}(\mathbf{x}_b - \boldsymbol{\mu}_b). \quad (18)$$

266 It is important to note that Σ_{bb}^{-1} in Equations (17) and (18) signifies
 267 the inverse of the covariance matrix Σ_{bb} . Thus, the conditional variance
 268 $\sigma_{a|b}^2$ essentially represents the Schur complement of Σ_{bb} within the overall
 269 covariance matrix Σ .

270 2.5. Gaussian Anomaly Detection

271 From a viewpoint of statistics, outliers are commonly denoted as values
 272 that significantly deviate from the mean. Under the assumption that the
 273 spatial and temporal characteristics of a system, observed over a moving
 274 window, can be suitably represented as normally distributed features, we
 275 assert that any anomaly can be identified as an outlier.

276 From a statistical viewpoint, outliers can be denoted as values that sig-
 277 nificantly deviate from the mean. Assuming that the spatial and temporal
 278 characteristics of the system over the moving window can be encoded as nor-
 279 mally distributed features, we can claim, that any anomaly may be detected
 280 as an outlier.

281 In empirical fields like machine learning, the three-sigma rule (3σ) pro-
 282 vides a framework for characterizing the region of a distribution within which
 283 normal values are expected to fall with high confidence. This rule renders
 284 approximately 0.265% of values in the distribution as anomalous.

285 The 3σ rule establishes the probability that any sample x_a of a random
 286 vector X lies within a given CDF over a semi-closed interval as the distance
 287 from the conditional mean $\mu_{a|b}$ of 3 conditional variances $\sigma_{a|b}^2$ and gives an
 288 approximate value of q as

$$q = P\{|x_a - \mu_{a|b}| < 3\sigma_{a|b}^2\} = 0.99735. \quad (19)$$

289 Utilizing a probabilistic model of normal behavior, we can determine
 290 threshold values x_l and x_u corresponding to the closed interval of the CDF

291 where this probability is established. The inversion of Equation (10) facilitates
 292 this calculation, yielding:

$$x_l = F((1 - P\{|x_a - \mu_{a|\mathbf{b}}| < 3\sigma_{a|\mathbf{b}}^2\}); \mu_{a|\mathbf{b}}, \sigma_{a|\mathbf{b}}^2)^{-1}, \quad (20)$$

293 for the lower limit, and

$$x_u = F((P\{|x_a - \mu_{a|\mathbf{b}}| < 3\sigma_{a|\mathbf{b}}^2\}); \mu_{a|\mathbf{b}}, \sigma_{a|\mathbf{b}}^2)^{-1}, \quad (21)$$

294 for the upper limit. These lower and upper limits together form vectors
 295 \mathbf{x}_l and \mathbf{x}_u , respectively, defining the region of normal system operation. This
 296 region is conceptualized as a hypercube in the feature space, with each di-
 297 mension bounded by the corresponding feature limits, as computed using
 298 Equations (20) and (21) for all $a = 1, \dots, k$; $\mathbf{b} = \{1, 2, \dots, k\}$ where $a \notin \mathbf{b}$.

299 Such threshold is computed for each feature of the system, resulting in
 300 a vector of lower and upper limits. The vector of limits is used to define
 301 the region of normal operation of the system. The region is defined as a
 302 hypercube in the feature space, where each dimension is defined by the limits
 303 of the corresponding feature.

304 The predicted state of the system, denoted as y_i , and the presence of
 305 anomalies in signals $\mathbf{y}_{s,i}$ at time i are determined based on the maximum
 306 distance of observations from the center of the hypercube. The center of the
 307 hypercube corresponds to the vector of conditional means $\mu_{a|\mathbf{b}}$ with respect
 308 to other features. The calculation of this distance involves the cumulative
 309 distribution function (CDF) of observations and conditional distributions, as
 310 follows:

$$F(x_a; \mu_{a|\mathbf{b}}, \sigma_{a|\mathbf{b}}^2) : a = 1, \dots, k; \mathbf{b} = \{1, 2, \dots, k\} \text{ where } a \notin \mathbf{b}. \quad (22)$$

311 Subsequently, anomalies in individual inputs are defined as follows:

$$\mathbf{y}_{s,i} = \begin{cases} 0 & \text{if } T \leq (22) \\ 1 & \text{if } T > (22), \end{cases} \quad (23)$$

312 where T represents a threshold that distinguishes between normal signal
 313 measurement ($\mathbf{y}_{s,i} = 0$) and abnormal ($\mathbf{y}_{s,i} = 1$).

314 For the predicted state of the system, the maximum value from $\mathbf{y}_{s,i}$ is
 315 considered, resulting in:

$$y_i = \begin{cases} 1 & \text{if } 1 \in \mathbf{y}_{s,i} \\ 0 & \text{otherwise,} \end{cases} \quad (24)$$

316 defining the discrimination boundary between system operation where
 317 $y_i = 0$ indicates normal system operation, and $y_i = 1$ indicates anomalous
 318 operation.

319 *2.6. Anomaly Definition*

320 In the realm of data analysis, anomalies are conspicuous deviations from
 321 the anticipated patterns within a dataset. Traditionally, the task of anomaly
 322 detection has relied upon unsupervised methodologies, wherein the identifi-
 323 cation of "outliers" entails the comparison of data points in both temporal
 324 and spatial contexts. This approach, often referred to as point-wise anomaly
 325 detection, classifies a data point as an anomaly when it exhibits significant
 326 dissimilarity from its neighboring data points (Iglesias Vázquez et al. (2023)).

327 The concept of point anomalies, influenced by factors such as temporal
 328 and spatial aspects, can be further categorized into conditional and contex-
 329 tual anomalies (Ruff et al. (2021)).

330 Nevertheless, this conventional method may not be suitable for scenarios
 331 characterized by collective anomalies, where clusters of abnormal data points
 332 coexist. A more pragmatic approach defines anomalies as deviations from
 333 established "normal" patterns, resembling the principles of semi-supervised
 334 learning. Change point detection, in a similar vein, can be regarded as a
 335 relative approach that takes into account the varying dynamics of changes,
 336 whether they occur gradually or abruptly (Iglesias Vázquez et al. (2023)).

337 It is imperative to recognize that the interpretation of anomalies, outliers,
 338 and novelties can vary upon the application. Anomalies typically garner
 339 significant attention, while outliers are often treated as undesirable noise
 340 and are typically excluded during data preprocessing. Novelties, on the other
 341 hand, signify new observations that necessitate model updates to adapt to
 342 an evolving environment (Ruff et al. (2021)).

343 Notwithstanding the differences in terminology, methods employed for the
 344 identification of data points residing in low-probability regions, irrespective
 345 of whether they are referred to as "anomaly detection," "outlier detection,"
 346 or "novelty detection," share fundamental similarities (Iglesias Vázquez et al.
 347 (2023)).

348 **3. Novelty Detection and Interpretation Framework**

349 In this section, we propose an adaptive and interpretable detection frame-
350 work for multivariate systems with streaming IoT devices. This approach
351 models the system as a dynamic joint normal distribution, enabling it to ef-
352 fectively adapt to pervasive nonstationary effects on processes. Our method
353 handles various factors, including change points, concept drift, and seasonal
354 effects. Our primary contribution lies in the fusion of an adaptable self-
355 supervised system with root cause identification capabilities. This combi-
356 nation empowers the online statistical model to diagnose anomalies through
357 two distinct avenues. Firstly, it employs conditional probability calculations
358 to assess the system’s operating conditions’ normality. Secondly, it identifies
359 outliers within individual signal measurements and features based on dy-
360 namic alert-triggering process limits. In the following sections, we describe
361 our proposed methodology across three subsections. The initial subsection
362 delves into the process of initializing the model’s parameters. The subsequent
363 section describes online training and adaptation, while the final subsection
364 expounds upon the model’s detection and diagnostic capabilities. For a con-
365 cise representation of the proposed method, Algorithm 2 is provided.

366 *3.1. Model Parameters Initialization*

367 The model initialization is governed by defining two tunable hyperparam-
368 eters of the model: the expiration period (t_e) and the threshold (T). The
369 expiration period determines the window size for time-rolling computations,
370 impacting the proportion of outliers within a given timeframe, and directly
371 influencing the relaxation (with a longer expiration period) or tightening
372 (with a shorter expiration period) of dynamic signal limits. Additionally, we
373 introduce a grace period, which defaults to $3/4t_e$, allowing for model calibra-
374 tion. During this grace period, system anomalies are not flagged to prevent
375 false positives and speed up self-supervised learning in Subsection 3.2. The
376 length of the expiration period inversely correlates with the model’s ability
377 to adapt to sudden changes. The adaptation to shifts in the data-generating
378 process, such as changes in mean or variance, is managed through the adapta-
379 tion period t_a . A longer t_a results in slower adaptation but potentially longer
380 alerts, which can be valuable during extended outlier periods. In most cases,
381 $t_a = 1/4t_e$ offers optimal performance.

382 As a general rule of thumb, expiration period t_e should be determined
383 based on the slowest observed dynamics within the multivariate system. The

384 threshold T defaults to the three-sigma probability of q in (19). Adjusting
 385 this threshold can fine-tune the trade-off between precision and recall. A
 386 higher threshold boosts recall but may lower precision, while a lower thresh-
 387 old enhances precision at the cost of recall. The presence of one non-default
 388 easily interpretable hyperparameter facilitates adaptability to various sce-
 389 narios. We recommend starting with the default values of other parameters
 390 and making adjustments based on real-time model performance.

391 *3.2. Online training*

392 Training in RAID follows an incremental learning approach, processing
 393 each new sample upon arrival. Incremental learning allows online parame-
 394 ter updates, albeit with a potential computational delay affecting response
 395 latency.

396 In the case of a dynamic joint probability distribution, the parameters are
 397 μ_i and Σ_i at time instance i . Update of the mean vector μ_i and covariance
 398 matrix Σ_i is governed by Welford's online algorithm using equation (2) and
 399 (4) respectively. Samples beyond the expiration period t_e are disregarded
 400 during the second pass. The effect of expired samples is reverted using inverse
 401 Welford's algorithm for mean (6) and variance (7), accessing the data in the
 402 buffer. For details, refer to Subsection 2.2.

403 It's worth noting that adaptation relies on two self-supervised methods.
 404 Adaptation routine runs if the observation at time instance i is considered
 405 normal. Adaptation period t_a allows the model to update the distribution
 406 on outliers as well. Given the predicted system anomaly state from (24) as
 407 y_i over the window of past observations $\mathbf{y}_i = \{y_{i-t_a}, \dots, y_i\}$, the following test
 408 holds when adaptation is performed on outlier:

$$\frac{\sum_{y \in \mathbf{y}_i} y}{n(\mathbf{y}_i)} > 2 * (T - 0.5). \quad (25)$$

409 Here $n(\mathbf{y}_i)$ denotes the dimensionality of \mathbf{y}_i . The logic of the (25) follows the
 410 probabilistic approach to anomalies that assumes a number of anomalies are
 411 lower or equal to the conditional probability at both tails of the distribution

412 *3.3. Online prediction*

413 In the prediction phase, multiple metrics are evaluated to assess the state
 414 of the modeled system.

415 Firstly, we calculate the parameters of the conditional distribution con-
 416 cerning the dynamic multivariate Gaussian distribution. These calculations

417 are performed for the process observation vector \mathbf{x}_i at time instance i . Specifically,
418 we compute the conditional mean using (18) and the conditional variance
419 using (17). These computations yield univariate conditional distributions
420 for individual signals and features. These conditional distributions play
421 a crucial role in assessing the abnormality of signals and features concerning
422 other observed values. This assessment relies on the strength of relationships
423 defined by the covariance matrix of the dynamic multivariate Gaussian
424 distribution. Consequently, our approach inherently considers the interactions
425 between input signals and features. The determination of anomalous
426 behavior is governed by (23).

427 Any anomaly detected within one of the features triggers an alert at the
428 system level. The decision regarding the overall system's anomalous behavior
429 is guided by (24). Nevertheless, individual determinations of anomalies serve
430 as a diagnostic tool for isolating the root cause of anomalies.

431 To assist operators in their assessments, we establish a hypercube defined
432 by lower and upper threshold values, denoted as \mathbf{x}_l and \mathbf{x}_u , respectively.
433 These thresholds are derived from (20) and (21), incorporating updated
434 model parameters. Lower and upper thresholds play a pivotal role as dynamic
435 process limits. They replace the conservative process limits provided
436 in sensor documentation, accounting for factors such as aging and actual
437 environmental conditions that influence sensor operation.

438 Our framework anticipates unexpected novel behavior, including signal
439 loss. This anticipation involves calculating the cumulative distribution function
440 (CDF) over the univariate normal distribution of sampling, focusing
441 on the differences between subsequent timestamps. We operate under the
442 assumption that, over the long term, the distribution of sampling times remains
443 stable. As a result, we employ a one-pass update mechanism utilizing
444 (2) and (4). To proactively detect subtle changes in sampling patterns,
445 self-supervised learning is employed, leveraging anomalies weighted by the
446 deviation from $(1 - F(x_i; \mu, \sigma^2))$ for training.

447 The system is vigilant in identifying change points. When the adaptation
448 test specified in (25) is satisfied, change points are flagged and isolated. This
449 initiation of change points triggers updates to the model, ensuring it adapts
450 to evolving data patterns effectively.

Algorithm 2 Online Detection and Identification Workflow

Input: expiration period t_e

Output: system anomaly y_i , signal anomalies $\mathbf{y}_{s,i}$, sampling anomaly $y_{t,i}$, change-point $y_{c,i}$, lower thresholds $\mathbf{x}_{l,i}$, upper thresholds $\mathbf{x}_{u,i}$,

Initialisation :

- 1: $i \leftarrow 1; n \leftarrow 1; T \leftarrow (19); \boldsymbol{\mu} \leftarrow \mathbf{x}_0; \boldsymbol{\Sigma} \leftarrow \mathbf{1}_{k \times k}; \mu_t \leftarrow 0; \sigma_t^2 \leftarrow 1;$
 - 2: compute $F(\mathbf{x}_0; \boldsymbol{\mu}, \boldsymbol{\Sigma})$ using algorithm in Genz (2000);
LOOP Process
 - 3: **loop**
 - 4: $\mathbf{x}_i, t_i \leftarrow \text{RECEIVE}();$
 - 5: $\mathbf{y}_{s,i} \leftarrow \text{PREDICT}(\mathbf{x}_i, T)$ using (23);
 - 6: $y_i \leftarrow \text{PREDICT}(\mathbf{y}_{s,i})$ using (24);
 - 7: $\mathbf{x}_{l,i}, \mathbf{x}_{u,i} \leftarrow \text{GET}(T, \boldsymbol{\mu}, \boldsymbol{\Sigma})$ using Algorithm 1;
 - 8: $y_{t,i} \leftarrow \text{PREDICT}(t_i - t_{i-1})$ using (23);
 - 9: $\mu_t, \sigma_t^2 \leftarrow \text{UPDATE}(t_i - t_{i-1}, \mu_t, \sigma_t^2)$ using (2), (4);
 - 10: **if** not (24) **or** (25) **then**
 - 11: $\boldsymbol{\mu}, \boldsymbol{\Sigma} \leftarrow \text{UPDATE}(\mathbf{x}_i, \boldsymbol{\mu}, \boldsymbol{\Sigma}, n)$ using (2), (4);
 - 12: **if** (25) **then**
 - 13: $y_{c,i} \leftarrow 1;$
 - 14: **else**
 - 15: $y_{c,i} \leftarrow 0;$
 - 16: **end if**
 - 17: $n \leftarrow n + 1;$
 - 18: **for** \mathbf{x}_{i-t_e} **do**
 - 19: $\boldsymbol{\mu}, \boldsymbol{\Sigma} \leftarrow \text{REVERT}(\mathbf{x}_{i-t_e}, \boldsymbol{\mu}, \boldsymbol{\Sigma}, n)$ using (6), (7);
 - 20: $n \leftarrow n - 1;$
 - 21: **end for**
 - 22: **end if**
 - 23: $i \leftarrow i + 1;$
 - 24: **end loop**
-

451 **4. Case Study**

452 This section provides a benchmark and two case studies that showcase
453 the effectiveness and applicability of our proposed approach. In the following
454 Subsections, we investigate the properties and performance of the approach
455 using streamed benchmark system data and signals from IoT devices in a mi-

456 crogrid system. The successful deployment demonstrates that this approach
457 is suitable for existing process automation infrastructure.

458 The case studies were realized using Python 3.10.1 on a machine employ-
459 ing an 8-core Apple M1 CPU and 8 GB RAM.

460 *4.1. Benchmark*

461 In this subsection, we compare the proposed method with adaptive un-
462 supervised detection methods without an interpretability layer. Two of the
463 well-established methods, providing iterative learning capabilities over mul-
464 tivariate time-series data are One-Class Support Vector Machine (OC-SVM)
465 and Half Spaced Trees (HS-Trees). Both methods represent the backbone
466 of multiple state-of-the-art methods for cases of anomaly detection on dy-
467 namic system data, with a brief list of recent applications in Introduction
468 1.3. Comparison is conducted on real benchmarking data, annotated with
469 labels of whether the observation was anomalous or normal. The dataset of
470 Skoltech Anomaly Benchmark (SKAB) Katser and Kozitsin (2020) is used for
471 this purpose, as no established benchmarking multivariate data were found
472 regarding energy storage systems. It represents a combination of experiments
473 with the behavior of rotor imbalance as a subject to various functions intro-
474 duced to control action as well as slow and sudden changes in the amount
475 of water in the circuit. The system is described by 8 features. The data
476 were preprocessed according to best practices for the given method, namely:
477 standard scaling for OC-SVM, normalization for HS-Trees, and no scaling
478 for our proposed method. The optimal quantile threshold value for both
479 reference methods is found using Bayesian Optimization. Due to no further
480 knowledge about the process, the parameters of the proposed method were
481 optimized using Bayesian Optimization as well. Results are provided within
482 Table 1, evaluating F1 score, Recall and Precision. A value of 100% at each
483 metric represents a perfect detection. The latency represents the average
484 computation time per sample of the pipeline including training and data
485 preprocessing.

486 The results in Table 1 suggest, that our algorithm provides slightly better
487 performance than reference methods. Based on the Scoreboard for various
488 algorithms on SKAB’s Kaggle page, our iterative approach performs com-
489 parably to the evaluated batch-trained model. Such a model has all the
490 training data available before prediction unlike ours, evaluating the metrics
491 iteratively on a streamed dataset.

Table 1: Metrics evaluation on SKAB dataset

Metric	AID	OC-SVM	HS-Trees
F1 [%]	48.70	44.42	34.10
Recall [%]	49.90	56.67	32.57
Precision [%]	47.56	36.52	35.77
Avg. Latency [ms]	1.55	0.44	0.21

492 *4.2. Battery Energy Storage System (BESS)*

493 In the first case study, we verify our proposed method on BESS. The
 494 BESS reports measurements of State of Charge (SoC), supply/draw energy
 495 set-points, and inner temperature, at the top, middle, and bottom of the
 496 battery module. Tight battery cell temperature control is needed to optimize
 497 performance and maximize the battery’s lifespan. Identifying anomalous
 498 events and removal of corrupted data might yield significant improvement
 499 in the process control level and increase the reliability and stability of the
 500 system.

501 The default sampling rate of the signal measurement is 1 minute. How-
 502 ever, network communication of the IoT devices is prone to packet dropout,
 503 which results in unexpected non-uniformities in sampling. The data are
 504 normalized to the range $[0, 1]$ to protect the sensitive business value. The
 505 proposed approach is deployed to the existing infrastructure of the system,
 506 allowing real-time detection and diagnosis of the system.

507 The industrial partner provided a physical model of the battery cell tem-
 508 perature, defined as follows:

$$\begin{aligned} T_{\text{bat},i+1} = & T_{\text{bat},i} + T_s(q_{\text{fan}}V_{\text{b,max}}\rho c_p(T_{\text{out}} - T_{\text{bat},i}) + V_{\text{c,max}}q_{\text{circ,fan}}\rho c_p T_{\text{bat},i} \\ & + q_{\text{circ,fan}}(P_{\text{cool}}q_{\text{cool}}P_{\text{heat}}q_{\text{heat}}) + c_{\text{scale}}Q_{\text{bat}} + q_{\text{inner fans}} \\ & - (V_{\text{b,max}}q_{\text{fan}}V_{\text{c,max}}q_{\text{circ,fan}})\rho c_p T_{\text{bat},i})/(m_{\text{bat}}c_{\text{p,b}}) \end{aligned} \quad (26)$$

509 When combined with an averaged measurement of battery cell temper-
 510 ature, we could compute the difference between real and predicted temper-
 511 ature. Such deviation can be useful in detecting unexpected patterns in
 512 temperature. Nevertheless, it may be inaccurate as the physical model is
 513 simplified and does not account for spatial aspects, like temperature gra-
 514 dients as well as different dynamic effects of charging and discharging on

515 temperature. Therefore, the raw measured temperature is used as well. The
516 deviation between demanded power and delivered power was used to aid the
517 identification of the state, as the increased difference might be related to
518 other unexpected and novel patterns.

519 Fig. 1 depicts the operation of the BESS over March 2022. Multiple
520 events of anomalous behavior happened within this period, confirmed by the
521 operators, that are observable through a sudden or significant shift in mea-
522 surements in a given period. As the first step, the detection mechanism was
523 initialized, following the provided guidelines for parameter selection in Sub-
524 section 3.1. The expiration period was set to $t_e = 7$ days, due to the weekly
525 seasonality of human behavior impacting battery usage. The threshold was
526 kept at default value $T = 0.99735$. A grace period, during which the model
527 learns from both normal and anomalous data (though normal are expected),
528 is shortened to 2.5 days to observe the effect of BESS calibration happening
529 on 3rd day from deployment.

530 The deployment and operation of the anomaly detection system were suc-
531 cessful as shown by its adaptation of changepoint on 7th March 2022 that
532 appeared due to the relocation of the battery storage system outdoors. The
533 model was adapted online based on Subsection 3.2. The sudden shift in envi-
534 ronmental conditions, due to the transfer of the system to outside changed the
535 dynamics of the system's temperature. However, new behavior was adopted
536 by the top-level anomaly isolation system within five days, reducing potential
537 false alerts afterward, by observably shifting the conditional mean to lower
538 temperatures. Perhaps more interesting are the alerted changepoints.

539 Calibration of the BESS, usually observed as deviations of setpoint from
540 real power demand and multiple peaks in temperature was captured as well.

541 The system identified 6 deviations in sampling, denoted by the red bars
542 in Fig. 1. 4 anomalies with shorter duration represented packet loss. The
543 prolonged anomaly was notified during the transfer of the battery pack. The
544 longest dropout observed happened across 20th March up to 21st. Unexpect-
545 edly, the change point detection module triggered an alarm at the end of
546 the loss, resulting in adaptation and a sharp shift in drawn limits for Power
547 Setpoint Deviation. Red dots represent anomalies at the signal level given
548 by equation (23). The dynamic signal limits are surpassed in one or multiple
549 signals during the system's anomalies. The root cause isolation allows the
550 pairing of anomalies with specific features. Conditional probability, against
551 which the anomalies are evaluated allows consideration of signal relationships
552 within individual limits.

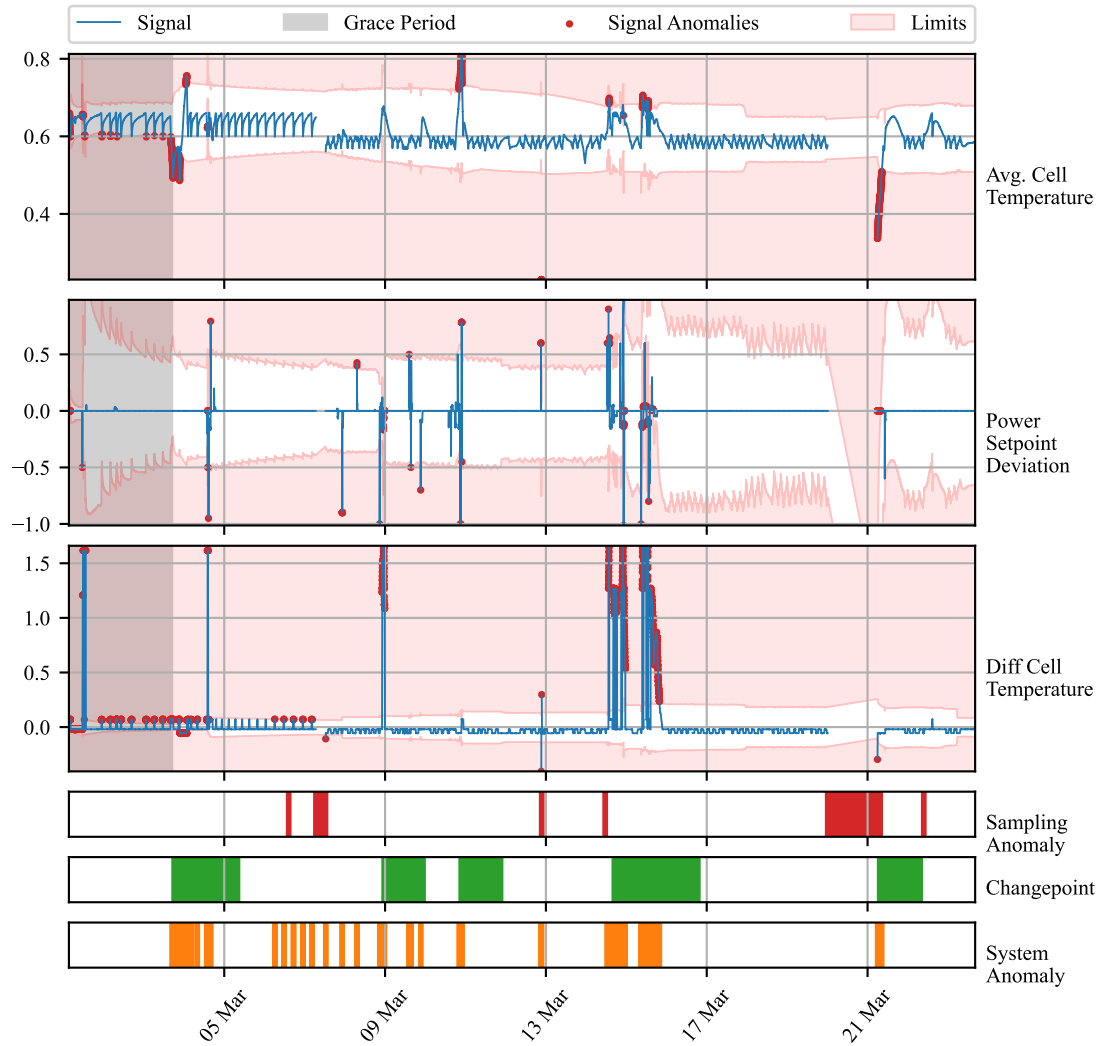


Figure 1: Time Series of BESS measurements (blue line) of process variables. The y-axis renders the values after the normalization of raw inputs. Root causes of anomalies are marked within specific signals as red dots. The light red area represents out-of-limits values for individual signals. Non-uniform sampling is marked as red bars. Green bars represent the times, at which changepoint was detected. All the signal anomalies are depicted as orange bars below the graph.

553 4.3. *Kokam Battery Temperature Module(BESS)*

554 A second case study is concerned with monitoring temperature profiles of
555 individual modules of battery pack deployed at end user. During the oper-
556 ation, a hardware fault of the cooling fan happened. Our industrial partner
557 was interested in finding out, whether such an event could be captured by
558 an anomaly detection system. The data for 12 modules, each coming with 6
559 channels of measurement were retrieved in 30-second sampling and processed
560 in a streamed manner. We found it informative to compute the deviation
561 of the observed value from the average of all the above-mentioned measure-
562 ments.

563 Our anomaly detection system was, once again, initialized with an ex-
564 piration period of 7 days. The grace period was shortened to 1 day. The
565 threshold value was shifted to a 4 sigma value of 99.977% to minimize the
566 number of alarms.

567 In Figure 2 we observe 5 days of deviations between the observed tem-
568 perature measured by channels of module 9 and the average temperature
569 of all modules. After the grace period, we observe multiple system alarms
570 raised by various channels. Until the noon of 22nd August, they seem to be
571 spread out randomly between individual channels. During the late evening
572 of 22nd, anomalies were reported by both channels 4 and 5 for a prolonged
573 period, followed by an anomalous rise in temperature measured by channel
574 6 early in the morning on 23rd August. The fan fault was observed approx-
575 imately at 5 pm on 23rd August. Our anomaly detection system instantly
576 raised an alarm, notifying us of anomalous behavior reported by channels 1
577 - 3. The prolonged duration of the alarm triggered the changepoint alarm
578 approximately 2 hours later. This resulted in a slightly faster adaptation of
579 the system to the new operation under increased temperature. Surprisingly,
580 the temperature decreased during the next day, notifying us of the fan being
581 in operation, to fail again 30 minutes later after the battery modules were
582 cooled down to the previous setpoint. The anomaly detection system was
583 triggered once again, although adaptation loosened the region of normal op-
584 eration to allow itself to adapt. No significant anomalies in sampling were
585 observed during the period.

586 **5. Conclusion**

587 In this paper, we examine the capacity of adaptive conditional probability
588 distribution to model the normal operation of dynamic systems employing

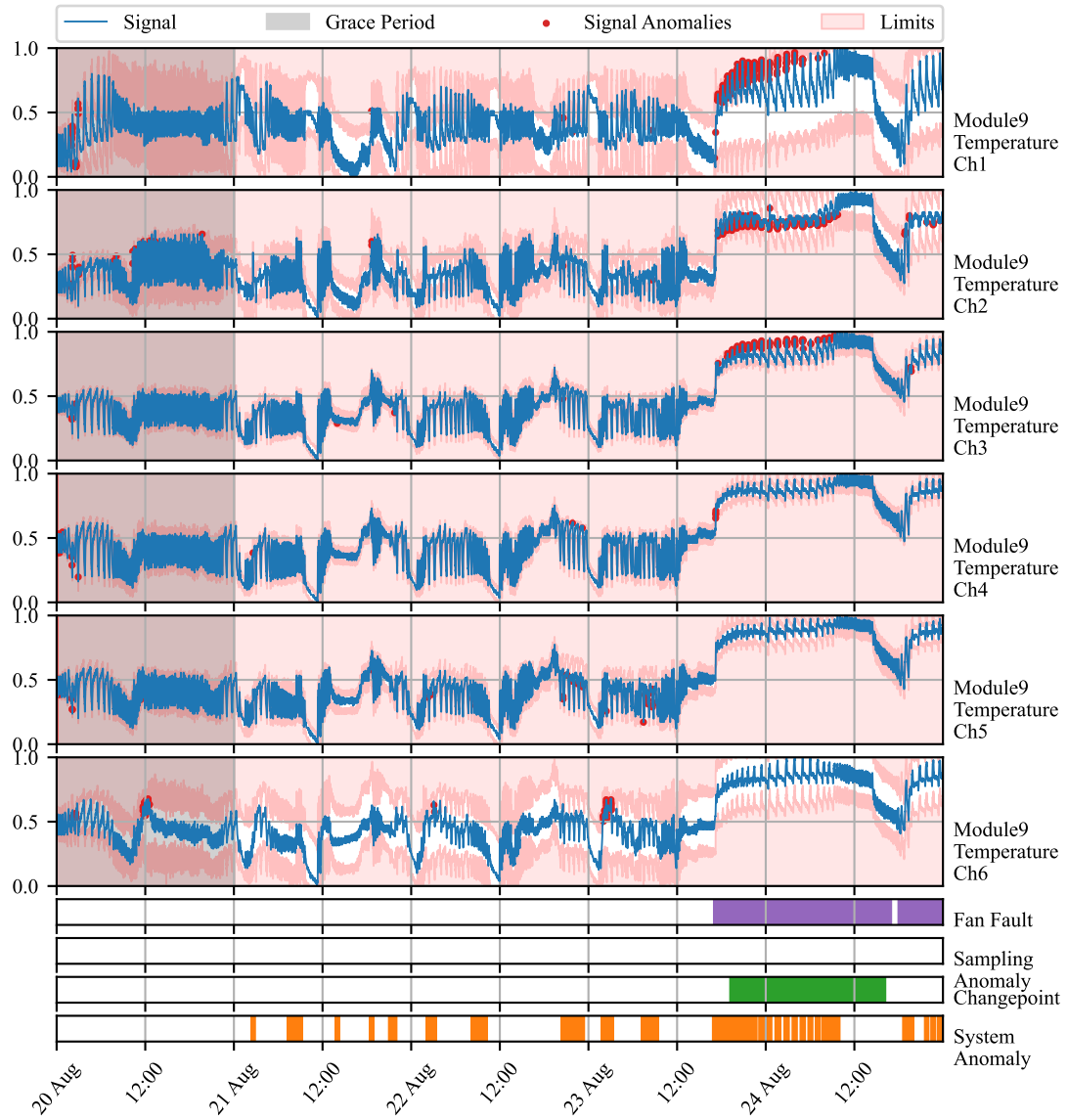


Figure 2: Time Series of BESS measurements (green line) of process variables. Non-uniform ticks on the x-axis mark days of interest (NOTE: some marks are hidden due to the readability). The y-axis renders the normalized process variables. System anomalies are marked as red dots. Non-uniform sampling is detected at blue vertical lines. Yellow vertical lines denote changepoint adaptation

589 streaming IoT devices and isolate the root cause. The dynamics of the sys-
590 tems are elaborated in the model using Welford’s online algorithm with the
591 capacity to update and revert sufficient parameters of underlying multivariate
592 Gaussian distribution in time making it possible to elaborate non-stationarity
593 in the process variables. Moreover, the self-supervision allows protection of
594 the distribution from the effect of outliers and increased speed of adaptation
595 in cases of changes in operation.

596 We assume the Gaussian distribution of measurements over a bounded
597 time frame related to the system dynamics. We consider such an assumption
598 reasonable, with support of multiple trials where the Kolmogorov-Smirnov
599 test did not reject this hypothesis. The statistical model provides the capac-
600 ity for the interpretation of the anomalies as extremely deviating observations
601 from the mean vector. Another assumption held in this study is that any
602 anomaly, spatial or temporal, can be transformed in such a way that makes
603 it an outlier given that we expose such effects as features as shown in case
604 studies.

605 Our approach establishes the system’s operation state at the global anomaly
606 level by considering interactions between input measurements and engineered
607 features and computing distance from mean of conditional probability. At
608 the second level, dynamic process limits based on PPF at threshold probabili-
609 ty, given multivariate distribution parameters, help isolate the root cause of
610 anomalies. This level serves the diagnostic purpose of the model operation.
611 The individual signals contribute to the global anomaly prediction, while
612 the proposed dynamic limits offer less conservative restrictions on individual
613 process operation. In parallel, the detector allows discrimination of signal
614 losses due to packet drops and sensor malfunctioning.

615 The ability to detect and identify anomalies in the system, isolate the
616 root cause of anomaly to specific signal or feature, and identify signal losses
617 is shown in two case studies on real data. Unlike many anomaly detec-
618 tion approaches, the proposed AID method does not require historical data
619 or ground truth information about anomalies, relieving general limitations.
620 Moreover, it combines adaptability and interpretability, which is an area yet
621 to be explored.

622 The benchmark performed on industrial data showed the ability to pro-
623 vide comparable results to other self-learning adaptable anomaly detection
624 methods. This is an important property for our model which allows, in
625 addition, the root cause isolation. The first case study, performed on real
626 operation data of BESS, examined the battery energy storage system and

627 demonstrated the ability to capture system anomalies and provide less con-
628 servative limits to signals. The physical model aided decisions about the
629 normality of the measured temperature of BESS.

630 The second case study exposed the ability to detect anomalies in the
631 temperature profiles of battery modules within the battery pack, consider-
632 ing spatial measurements made by multiple sensors distributed around the
633 module and the average temperature of all the modules within the pack.
634 Hardware fault observed on this deployed device was captured by our model,
635 giving another proof of its importance in energy storage systems monitoring,
636 where tight temperature control plays a significant role in the safety and
637 profitability of the system.

638 Future works on the method will include improvement to the change point
639 detection mechanism, decrease in the latency on high dimensional data, and
640 false positive rate reduction, from which general plug-and-play models suffer.

641 References

642 V. Chandola, A. Banerjee, V. Kumar, Anomaly detection: A survey, ACM
643 Comput. Surv. 41 (2009). URL: <https://doi.org/10.1145/1541880.1541882>. doi:10.1145/1541880.1541882.

645 N. Laptev, S. Amizadeh, I. Flint, Generic and scalable framework for auto-
646 mated time-series anomaly detection, in: Proceedings of the 21th ACM
647 SIGKDD International Conference on Knowledge Discovery and Data Min-
648 ing, KDD '15, Association for Computing Machinery, New York, NY,
649 USA, 2015, pp. 1939–1947. URL: <https://doi.org/10.1145/2783258.2788611>. doi:10.1145/2783258.2788611.

651 A. Kejariwal, Introducing practical and robust anomaly
652 detection in a time series, 2015. URL: https://blog.twitter.com/engineering/en_us/a/2015/introducing-practical-and-robust-anomaly-detection-in-a-time-series.

655 A. A. Cook, G. Misirli, Z. Fan, Anomaly detection for iot time-series data:
656 A survey, IEEE Internet of Things Journal 7 (2020) 6481–6494. doi:10.
657 1109/JIOT.2019.2958185.

658 K. Zhang, J. Chen, C.-G. Lee, S. He, An unsupervised spa-
659 tiotemporal fusion network augmented with random mask and time-
660 relative information modulation for anomaly detection of machines

- 661 with multiple measuring points, Expert Systems with Applications 237 (2024) 121506. URL: <https://www.sciencedirect.com/science/article/pii/S0957417423020080>. doi:<https://doi.org/10.1016/j.eswa.2023.121506>.
- 665 J. Huang, D. Cheng, S. Zhang, A novel outlier detecting algorithm based on the outlier turning points, Expert Systems with Applications 231 (2023) 120799. URL: <https://www.sciencedirect.com/science/article/pii/S0957417423013015>. doi:<https://doi.org/10.1016/j.eswa.2023.120799>.
- 670 C. Fan, Y. Sun, Y. Zhao, M. Song, J. Wang, Deep learning-based feature engineering methods for improved building energy prediction, Applied Energy 240 (2019) 35–45. URL: <https://www.sciencedirect.com/science/article/pii/S0306261919303496>. doi:<https://doi.org/10.1016/j.apenergy.2019.02.052>.
- 675 P. D. Talagala, R. J. Hyndman, K. Smith-Miles, Anomaly detection in high-dimensional data, Journal of Computational and Graphical Statistics 30 (2021) 360–374. URL: <https://doi.org/10.1080/10618600.2020.1807997>. doi:<https://doi.org/10.1080/10618600.2020.1807997>. arXiv:<https://doi.org/10.1080/10618600.2020.1807997>.
- 680 J. Li, Z. Liu, Attribute-weighted outlier detection for mixed data based on parallel mutual information, Expert Systems with Applications 236 (2024) 121304. URL: <https://www.sciencedirect.com/science/article/pii/S0957417423018067>. doi:<https://doi.org/10.1016/j.eswa.2023.121304>.
- 685 X. Du, J. Chen, J. Yu, S. Li, Q. Tan, Generative adversarial nets for unsupervised outlier detection, Expert Systems with Applications 236 (2024) 121161. URL: <https://www.sciencedirect.com/science/article/pii/S0957417423016639>. doi:<https://doi.org/10.1016/j.eswa.2023.121161>.
- 690 M. Salehi, L. Rashidi, A survey on anomaly detection in evolving data: [with application to forest fire risk prediction], SIGKDD Explor. Newsl. 20 (2018) 13–23. URL: <https://doi.org/10.1145/3229329.3229332>. doi:<https://doi.org/10.1145/3229329.3229332>.

- 694 N. Barbosa Roa, L. Travé-Massuyès, V. H. Grisales-Palacio, Dy-
695 clee: Dynamic clustering for tracking evolving environments, Pat-
696 tern Recognition 94 (2019) 162–186. URL: <https://www.sciencedirect.com/science/article/pii/S0031320319301992>. doi:<https://doi.org/10.1016/j.patcog.2019.05.024>.
- 699 A. G. Tartakovsky, A. S. Polunchenko, G. Sokolov, Efficient computer net-
700 work anomaly detection by changepoint detection methods, IEEE Journal
701 of Selected Topics in Signal Processing 7 (2013) 4–11. doi:[10.1109/JSTSP.2012.2233713](https://doi.org/10.1109/JSTSP.2012.2233713).
- 703 H. Wu, J. He, M. Tömösközi, Z. Xiang, F. H. Fitzek, In-network processing
704 for low-latency industrial anomaly detection in softwarized networks, in:
705 2021 IEEE Global Communications Conference (GLOBECOM), 2021, pp.
706 01–07. doi:[10.1109/GLOBECOM46510.2021.9685489](https://doi.org/10.1109/GLOBECOM46510.2021.9685489).
- 707 H. S. Pannu, J. Liu, S. Fu, Aad: Adaptive anomaly detection system for cloud
708 computing infrastructures, in: 2012 IEEE 31st Symposium on Reliable
709 Distributed Systems, 2012, pp. 396–397. doi:[10.1109/SRDS.2012.3](https://doi.org/10.1109/SRDS.2012.3).
- 710 S. Ahmad, A. Lavin, S. Purdy, Z. Agha, Unsupervised real-time anomaly
711 detection for streaming data, Neurocomputing 262 (2017) 134–
712 147. URL: <https://www.sciencedirect.com/science/article/pii/S0925231217309864>. doi:<https://doi.org/10.1016/j.neucom.2017.04.070>, online Real-Time Learning Strategies for Data Streams.
- 715 H. H. Bosman, G. Iacca, A. Tejada, H. J. Wörtche, A. Liotta, Ensembles
716 of incremental learners to detect anomalies in ad hoc sensor networks,
717 Ad Hoc Networks 35 (2015) 14–36. URL: <https://www.sciencedirect.com/science/article/pii/S1570870515001481>. doi:<https://doi.org/10.1016/j.adhoc.2015.07.013>, special Issue on Big Data Inspired Data
718 Sensing, Processing and Networking Technologies.
- 721 M. Carletti, C. Masiero, A. Beghi, G. A. Susto, Explainable machine learning
722 in industry 4.0: Evaluating feature importance in anomaly detection to
723 enable root cause analysis, in: 2019 IEEE International Conference on
724 Systems, Man and Cybernetics (SMC), 2019, pp. 21–26. doi:[10.1109/SMC.2019.8913901](https://doi.org/10.1109/SMC.2019.8913901).

- 726 Q. P. Nguyen, K. W. Lim, D. M. Divakaran, K. H. Low, M. C. Chan, Gee: A
727 gradient-based explainable variational autoencoder for network anomaly
728 detection, in: 2019 IEEE Conference on Communications and Network
729 Security (CNS), 2019, pp. 91–99. doi:10.1109/CNS.2019.8802833.
- 730 K. Amarasinghe, K. Kenney, M. Manic, Toward explainable deep neural
731 network based anomaly detection, in: 2018 11th International Conference
732 on Human System Interaction (HSI), 2018, pp. 311–317. doi:10.1109/HSI.
733 2018.8430788.
- 734 X. Zhang, J. Shi, X. Huang, F. Xiao, M. Yang, J. Huang,
735 X. Yin, A. Sohail Usmani, G. Chen, Towards deep probabilistic
736 graph neural network for natural gas leak detection and localiza-
737 tion without labeled anomaly data, Expert Systems with Appli-
738 cations 231 (2023) 120542. URL: <https://www.sciencedirect.com/science/article/pii/S0957417423010448>. doi:<https://doi.org/10.1016/j.eswa.2023.120542>.
- 741 W.-T. Yang, M. S. Reis, V. Borodin, M. Juge, A. Roussy, An interpretable
742 unsupervised bayesian network model for fault detection and diagno-
743 sis, Control Engineering Practice 127 (2022) 105304. URL: <https://www.sciencedirect.com/science/article/pii/S0967066122001502>.
744 doi:<https://doi.org/10.1016/j.conengprac.2022.105304>.
- 746 L. C. Brito, G. A. Susto, J. N. Brito, M. A. V. Duarte, Fault diagno-
747 sis using explainable ai: A transfer learning-based approach for rotating
748 machinery exploiting augmented synthetic data, Expert Systems with
749 Applications 232 (2023) 120860. URL: <https://www.sciencedirect.com/science/article/pii/S0957417423013623>. doi:<https://doi.org/10.1016/j.eswa.2023.120860>.
- 752 Z. Wu, X. Yang, X. Wei, P. Yuan, Y. Zhang, J. Bai, A self-supervised
753 anomaly detection algorithm with interpretability, Expert Systems with
754 Applications 237 (2024) 121539. URL: <https://www.sciencedirect.com/science/article/pii/S0957417423020419>. doi:<https://doi.org/10.1016/j.eswa.2023.121539>.
- 757 M. Wadinger, M. Kvasnica, Real-time outlier detection with dynamic pro-
758 cess limits, in: Proceedings of the 2023 24th International Conference on
759 Process Control (PC), 2023. In press.

- 760 K. Yamanishi, J.-i. Takeuchi, A unifying framework for detecting outliers and
761 change points from non-stationary time series data, in: Proceedings of the
762 Eighth ACM SIGKDD International Conference on Knowledge Discovery
763 and Data Mining, KDD '02, Association for Computing Machinery, New
764 York, NY, USA, 2002, pp. 676–681. URL: <https://doi.org/10.1145/775047.775148>. doi:10.1145/775047.775148.
- 765
- 766 K. Yamanishi, J.-i. Takeuchi, G. Williams, P. Milne, On-line unsu-
767 pervised outlier detection using finite mixtures with discounting learn-
768 ing algorithms, *Data Mining and Knowledge Discovery* 8 (2004) 275–
769 300. URL: <https://doi.org/10.1023/B:DAMI.0000023676.72185.7c>.
770 doi:10.1023/B:DAMI.0000023676.72185.7c.
- 771
- 772 B. Steenwinckel, Adaptive anomaly detection and root cause analysis by fus-
773 ing semantics and machine learning, in: A. Gangemi, A. L. Gentile, A. G.
774 Nuzzolese, S. Rudolph, M. Maleshkova, H. Paulheim, J. Z. Pan, M. Alam
775 (Eds.), *The Semantic Web: ESWC 2018 Satellite Events*, Springer Interna-
776 tional Publishing, Cham, 2018, pp. 272–282.
- 777
- 778 B. Steenwinckel, D. De Paepe, S. Vanden Hautte, P. Heyvaert, M. Ben-
779 tefrit, P. Moens, A. Dimou, B. Van Den Bossche, F. De Turck, S. Van
780 Hoecke, F. Ongena, Flags: A methodology for adaptive anomaly
781 detection and root cause analysis on sensor data streams by fusing
782 expert knowledge with machine learning, *Future Generation Com-
783 puter Systems* 116 (2021) 30–48. URL: <https://www.sciencedirect.com/science/article/pii/S0167739X20329927>. doi:<https://doi.org/10.1016/j.future.2020.10.015>.
- 784
- 785 M. Amer, M. Goldstein, S. Abdennadher, Enhancing one-class support vec-
786 tor machines for unsupervised anomaly detection, in: Proceedings of the
787 ACM SIGKDD Workshop on Outlier Detection and Description, ODD '13,
788 Association for Computing Machinery, New York, NY, USA, 2013, pp.
789 8–15. URL: <https://doi.org/10.1145/2500853.2500857>. doi:10.1145/2500853.2500857.
- 790
- 791 B. Liu, Y. Xiao, P. S. Yu, L. Cao, Y. Zhang, Z. Hao, Uncertain one-class
792 learning and concept summarization learning on uncertain data streams,
793 *IEEE Transactions on Knowledge and Data Engineering* 26 (2014) 468–
794 484. doi:10.1109/TKDE.2012.235.

- 794 B. Krawczyk, M. Woźniak, One-class classifiers with incremental
795 learning and forgetting for data streams with concept drift, Soft
796 Computing 19 (2015) 3387–3400. URL: <https://doi.org/10.1007/s00500-014-1492-5>. doi:10.1007/s00500-014-1492-5.
- 798 X. Miao, Y. Liu, H. Zhao, C. Li, Distributed online one-class support vec-
799 tor machine for anomaly detection over networks, IEEE Transactions on
800 Cybernetics 49 (2019) 1475–1488. doi:10.1109/TCYB.2018.2804940.
- 801 Ö. Gözüaçık, F. Can, Concept learning using one-class classifiers for
802 implicit drift detection in evolving data streams, Artificial Intelli-
803 gence Review 54 (2021) 3725–3747. URL: <https://doi.org/10.1007/s10462-020-09939-x>. doi:10.1007/s10462-020-09939-x.
- 805 R. Wetzig, A. Gulenko, F. Schmidt, Unsupervised anomaly alerting for
806 iot-gateway monitoring using adaptive thresholds and half-space trees,
807 in: 2019 Sixth International Conference on Internet of Things: Systems,
808 Management and Security (IOTSMS), 2019, pp. 161–168. doi:10.1109/IOTSMS48152.2019.8939201.
- 810 Y. Lyu, W. Li, Y. Wang, S. Sun, C. Wang, Rmhsforest: Rel-
811 ative mass and half-space tree based forest for anomaly detec-
812 tion, Chinese Journal of Electronics 29 (2020) 1093–1101. URL:
813 <https://ietresearch.onlinelibrary.wiley.com/doi/abs/10.1049/cje.2020.09.010>.
814 doi:<https://doi.org/10.1049/cje.2020.09.010>.
815 arXiv:<https://ietresearch.onlinelibrary.wiley.com/doi/pdf/10.1049/cje.2020.09.010>
- 816 B. P. Welford, Note on a method for calculating corrected
817 sums of squares and products, Technometrics 4 (1962) 419–
818 420. URL: <https://www.tandfonline.com/doi/abs/10.1080/00401706.1962.10490022>.
819 doi:10.1080/00401706.1962.10490022.
820 arXiv:<https://www.tandfonline.com/doi/pdf/10.1080/00401706.1962.10490022>.
- 821 A. Genz, Numerical computation of multivariate normal probabilities, Jour-
822 nal of Computational and Graphical Statistics 1 (2000). doi:10.1080/
823 10618600.1992.10477010.
- 824 R. P. Brent, Algorithms for minimization without derivatives, Prentice-Hall,
825 Englewood Cliffs, N.J, 1972. URL: https://openlibrary.org/books/OL4739237M/Algorithms_for_minimization_without_derivatives.

827 F. Iglesias Vázquez, A. Hartl, T. Zseby, A. Zimek, Anomaly detection in
828 streaming data: A comparison and evaluation study, Expert Systems with
829 Applications 233 (2023) 120994. URL: <https://www.sciencedirect.com/science/article/pii/S0957417423014963>. doi:<https://doi.org/10.1016/j.eswa.2023.120994>.

832 L. Ruff, J. R. Kauffmann, R. A. Vandermeulen, G. Montavon, W. Samek,
833 M. Kloft, T. G. Dietterich, K.-R. Müller, A unifying review of deep and
834 shallow anomaly detection, Proceedings of the IEEE 109 (2021) 756–795.
835 doi:[10.1109/JPROC.2021.3052449](https://doi.org/10.1109/JPROC.2021.3052449).

836 I. D. Katser, V. O. Kozitsin, Skoltech anomaly benchmark (skab),
837 <https://www.kaggle.com/dsv/1693952>, 2020. doi:[10.34740/KAGGLE/DSV/1693952](https://doi.org/10.34740/KAGGLE/DSV/1693952).